Distributed Dynamic Coordination Control for Offshore Platform Transportation Under Ocean Environmental Disturbances

Du, Zhe; Negenborn, Rudy R.; Reppa, Vasso

DOI
10.1109/TCST.2023.3291557

Publication date
2023

Document Version
Final published version

Published in
IEEE Transactions on Control Systems Technology

Distributed Dynamic Coordination Control for Offshore Platform Transportation Under Ocean Environmental Disturbances

Zhe Du, Rudy R. Negenborn, and Vasso Reppa, *Member, IEEE*

***Abstract*— Transportation of a large offshore platform from inland waters to the open sea is a hazardous and challenging mission. With the development of the autonomous surface vessel (ASV), the problem of large floating object transportation has a chance to be solved by applying multiple physical-connected autonomous tugboats. This article proposes a distributed dynamic coordination control scheme for a multivessel autonomous towing system to transport an offshore platform under environmental disturbances. Where the dynamic coordination decision mechanism is based on the relative position of the two neighbor waypoints, the controllers are designed based on the multilayer model-predictive control (MPC) strategy with several specific cost functions, and the distributed control architecture is built based on the alternating direction method of multipliers (ADMM) with augmented Lagrangian function. The simulation experiment indicates that the proposed control scheme can achieve better consensus for the distributed control architecture accomplishment and more efficiently transport an offshore platform under environmental disturbances.**

***Index Terms*— Distributed model-predictive control (MPC), dynamic coordination control, environmental disturbances, multivessel system, offshore platform transportation.**

I. Introduction

THE requirement for ocean resources such as renewable energy (wind power, tidal and wave energy) [1], fishery and aquaculture industry [2], and seabed minerals [3] motivate the establishment of offshore platforms and the development of maritime transport services [4]. However, manipulating a large offshore platform from inland waters to the open sea is a hazardous and challenging mission. Such a problem is called large floating object transportation.

In recent decades, the rapid development of the autonomous surface vessels (ASVs) has extended its application from the case of single vessel simple tasks to multivessel system comprehensive missions [5], which enables the ASV to involve more complex and dangerous maritime operations. Hence, the problem of large floating object transportation can be solved by applying multiple physical-connected autonomous tugboats.

Solutions for large floating object transportation by ASVs can be classified into two categories according to the type of connection: attaching and towing, as seen in Table I. The first category is based on the technology of cooperative object transport by multirobot systems (MRSs). The strategies in the MRS object transport research consist of pushing-only, grasping, and caging manipulations. Considering the dynamic environments of the water surface, the idea of grasping strategy is used in the maritime field to make sure the connection is tight and stable between the manipulated object and the vessels. Thus, the attached manipulation means that each ASV attaches to the surface of the large floating object tightly.

To keep the balance for the floating object on the horizontal plane, the number of ASV is usually even. In research work [6], six ASVs attach to a distressed ship, the decentralized control strategy is based on optimal and feedback control combining Lyapunov theory. Bidikli et al. [7] also take advantage of six ASVs for ship dynamic positioning, where the decentralized robust controller is designed based on the feedback control law and the Lyapunov theory. Bui et al. [8] use the redistributed pseudo-inverse algorithm, which is based on the optimization method, and the Lyapunov theory to achieve a task of ship berthing by four ASVs. Lee et al. [9] combine sliding mode control and genetic optimization algorithm for four attached tugboats to convey a large surface vessel in the shipyard. Besides the even number of ASVs, Chen et al. [10] use three ASVs to cooperatively transport a floating object, where two ASVs are symmetrically located on the two sides and one ASV attaches at the stern of the object. Since this research focuses on the water transportation level (macro level), all the models used are linearized. Rosario et al. [11] design a sliding mode controller for a boat to push a floating load in which the contact point is free of slipping.

The attached manipulation is limited to applying in port areas with fewer environmental disturbances. When the disturbances have significant effects, the towed-based manipulation, which is closer to the common practice in maritime, is more investigated. The towing manipulation implies that each ASV is connected to the floating object by a towing line.

Manuscript received 28 June 2022; revised 10 December 2022 and 26 February 2023; accepted 15 March 2023. Date of publication 18 July 2023; date of current version 18 August 2023. This work was supported in part by the China Scholarship Council under Grant 201806950080, in part by the Researchlab Autonomous Shipping (RAS) of Delft University of Technology, in part by the EFRO REACT-EU Op-Zuid Project "Fieldlab Autonomous Sailing Technology (FAST)" under Grant 4119, and in part by the European Regional Development Fund through the INTERREG North Sea Region Grant "AVATAR." Recommended by Associate Editor M. Mammarella. *(Corresponding author: Zhe Du.)*

The authors are with the Department of Maritime and Transport Technology, Delft University of Technology, 2628 CD Delft, The Netherlands (e-mail: duzhe@whut.edu.cn; R.R.Negenborn@tudelft.nl; V.Reppa@tudelft.nl).

Color versions of one or more figures in this article are available at https://doi.org/10.1109/TCST.2023.3291557.

Digital Object Identifier 10.1109/TCST.2023.3291557

TABLE I
CLASSIFICATION OF LARGE FLOATING OBJECT TRANSPORTATION BY MULTIPLE ASVS

Research Article	Type of Connection	Number of ASV	Control Method*	Control Architecture	Disturbances Handling	Role of each ASV
[6]	Attaching	6	FBC + OC + LT	Distributed	Bounded forces	Propelling $\times 6$
[7]	Attaching	6	FBC + LT	Distributed	Bounded forces	Propelling $\times 6$
[8]	Attaching	4	OC + LT	Distributed	None	Propelling $\times 4$
[9]	Attaching	4	OC + SMC	Centralized	Wind and current forces	Propelling $\times 4$
[10]	Attaching	3	MPC	Distributed	None	Propelling $\times 3$
[11]	Attaching	1	SMC	Centralized	Fixed external forces	Propelling $\times 1$
[13]	Towing	1	PID	Centralized	Winds, Waves, Currents	Guiding $\times 1$
[14]	Towing	1	LADRC + RL	Centralized	Winds, Waves	Guiding $\times 1$
[15]	Towing	1	LADRC + PID	Centralized	Winds, Currents	Guiding $\times 1$
[16]	Towing	2	BSC	Distributed	Unmodeled disturbances	Guiding $\times 2$
[17]	Towing	2	MPC	Distributed	None	Guiding $\times 1$; Following $\times 1$
[18]	Towing	2	OC	Centralized	Winds, Waves	Guiding $\times 1$; Following $\times 1$
[19]	Towing	4	CC	Distributed	Winds, Waves, Currents	Guiding $\times 4$
[20]	Towing	4	DSC + OC +RC	Distributed	None	Guiding $\times 4$
This paper	**Towing**	**4**	**MPC**	**Distributed**	**Winds, Waves, Currents**	**Flexible** $\times 4$

* BSC: Backstepping Control; CC: Consensus Control; DSC: Dynamic Surface Control; FBC: Feedback Control; LADRC: Linear Active Disturbance Rejection Control; LT: Lyapunov Theory; MPC: Model Predictive Control; OC: Optimal-based Control; PID: Proportional Integral Derivative; RC: Robust Control; RL: Reinforcement Learning; SMC: Sliding Model Control.

Compared with the attached manipulation, this operation gives more freedom to the ASVs and reserves a safe distance between the ASVs and the manipulated floating object [12]. Thus, it is more preferred in the harsh and complex water environment.

In [13], a PID-based two-layer control strategy is proposed for a two-ship ensemble towing system that first maintaining a prescribed heading angle and surge speed, and then tracking the set targets. Zheng et al. [14] focus on the course keeping of a drilling platform towing system by designing a reinforcement learning-based linear active disturbance rejection control method. Tao et al. [15] combine the PID and linear active disturbance rejection control method for path following of a towing system of a cylindrical drilling platform. In [16], an extended backstepping control method is proposed to cooperate with two ASVs to manipulate a large buoyant load along a desired trajectory. Du et al. [17] propose a distributed model-predictive control (MPC)-based scheme for a towing system to manipulate a ship for desired position and heading, meanwhile following the recommended speed profiles. Du et al. [18] propose an optimization-based multiagent control algorithm for two autonomous tugboats to cooperatively manipulate a ship in port areas under environmental disturbances. Ianagui and Tannuri [19] propose a control method by introducing a virtual consensus leader to coordinate the motions of the four-ASV floating load system for set-point control. In [20], a robust cooperative trajectory tracking control is devised for a four-tugboat towing system based on the dynamic surface control technique.

On the one hand, floating object transportation systems are characterized by multiple control inputs and multiple control constraints. As can be noticed from Table I, the optimization-based control strategy, like the optimal control and the MPC, is preferred to address the floating object transportation problem. On the other hand, since the maneuverability of the floating object transportation system is often quite limited, in some scenarios like the system requiring large steering, the long response time of the control order will reduce the safety of the towing system. Thus, a predictive optimization-based control strategy (e.g., MPC) is more suitable for tackling this kind of problem.

From the viewpoint of control architecture, the control of multiple ASVs usually employs a distributed architecture, because it has better scalability and failures-tolerance when applied with multiagent systems [21]. As for disturbances, researchers studying the attaching systems tends to use bounded external forces for the environmental effects on the system; but for the towing systems, to represent the practical scenarios, the winds, waves, and currents disturbance model are often built.

The role of each ASV in a floating object transportation system is related to the type of connection. For the attaching system, every ASV performs propelling role to provide pushing force to the floating object [as shown in Fig. 1(a)]. For the towing system, the roles are determined by the number and the configuration of ASVs. In the case of one ASV, its role is usually a guiding tugboat [13], [14], [15] [as shown in Fig. 1(b), tugboat I]. For the case of two ASVs, if both

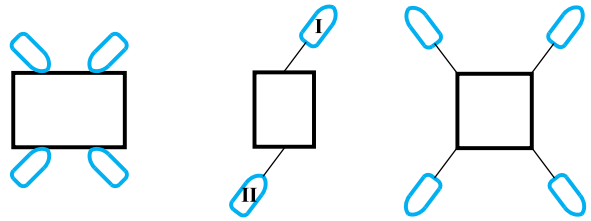

Fig. 1. Different cases of vessel role: the black box stands for the floating object, the blue one is the ASV (tugboat). (a) All tugboats play propelling role. (b) Tugboat I plays the guiding role and Tugboat II plays the following role. (c) All tugboats play the guiding role.

ASVs are in front of the object, they are regarded as guiding tugboats [16]; if the floating object is located between the two ASVs, the front ASV is the guiding tugboat, the rear ASV is the following tugboat [17], [18] [as shown in Fig. 1(b), tugboat I and II]. For the case of more than two ASVs, the role of every ASV is usually a guiding tugboat in different directions [19], [20] [as shown in Fig. 1(c)]. The object with more than two ASVs towing systems would often have better maneuverability. However, in this configuration [see Fig. 1(c)], the direction of at least two ASVs is in opposite direction to the goal in the process of towing. This could change the hydrodynamic parameters of these ASVs, as the hydrodynamic parameters of the vessel's model are calculated based on the motion of heading forward (except for the case of tugboats with Voith Schneider Propellers). Thus, this case of towing could result in model uncertainty problems.

Overall, compared with the attached manipulation (especially [10]), the towed-based manipulation provides better safety for the multiple ASVs and the floating object, which is more suitable considering the influence of environmental disturbances (which are not considered in [10]). To increase the efficiency of the towing process and improve the flexibility of each ASV while not changing its dynamics characters, it is important to develop a dynamic coordination control scheme to cope with different scenarios. In previous work, the authors have investigated the dynamic coordination control of multiple autonomous tugboats with flexible roles for offshore platform transportation [22]. However, in that work, the control architecture is centralized and the environmental disturbances are not considered. Therefore, the goal and the main contribution of this work is to propose a distributed dynamic coordination control scheme for a multi-ASV towing system to efficiently transport an offshore platform under ocean environmental disturbances.

The remainder of this article is organized as follows. Section II formulates the main problem, kinematics, and kinetics model of the towing system. The design of the proposed control scheme and the definition of a set of key performance indicators are given in Section III. In Section IV, simulation experiments are carried out for representative situations to illustrate the potential of the proposed scheme. Conclusions and future research directions are given in Section V.

II. Problem Statement

The objective of this work is to efficiently transport an offshore platform using four autonomous tugboats under ocean environmental disturbances. The motion of the platform and tugboats is formulated by the three-degree of freedom (DoF) hydrodynamic model [23], where the kinematics and kinetics formulations are expressed as

$$\dot{\boldsymbol{\eta}}_*(t) = \boldsymbol{R}(\psi_*(t))\boldsymbol{\nu}_*(t) \tag{1}$$

$$\begin{aligned}\boldsymbol{M}_*\dot{\boldsymbol{\nu}}_*(t) + \boldsymbol{C}_*(\boldsymbol{\nu}_*(t))\boldsymbol{\nu}_*(t) + \boldsymbol{D}_*\boldsymbol{\nu}_*(t)\\ = \boldsymbol{\tau}_*(t) + \boldsymbol{\tau}_{*\text{wind}}(t) + \boldsymbol{\tau}_{*\text{wave}}(t)\end{aligned} \tag{2}$$

where $*$ stands for O (offshore platform) or I (tugboat, $I \in \{\text{A}, \text{B}, \text{C}, \text{D}\}$); $\boldsymbol{\eta}_*(t) = [x_*(t)\ y_*(t)\ \psi_*(t)]^{\text{T}} \in \mathbb{R}^3$ is the position vector in the world frame (North-East-Down) including position coordinates $[x_*(t), y_*(t)]$ and heading $\psi_*(t)$; $\boldsymbol{\nu}_*(t) = [u_*(t)\ v_*(t)\ r_*(t)]^{\text{T}} \in \mathbb{R}^3$ is the velocity vector in the body-fixed frame containing the velocity of surge $u_*(t)$, sway $v_*(t)$, and yaw $r_*(t)$; $\boldsymbol{R} \in \mathbb{R}^{3\times3}$ is the rotation matrix from the body frame to the world frame, which is a function of heading; $\boldsymbol{M}_* \in \mathbb{R}^{3\times3}$, $\boldsymbol{C}_* \in \mathbb{R}^{3\times3}$, and $\boldsymbol{D}_* \in \mathbb{R}^{3\times3}$ are the mass (inertia), Coriolis-Centripetal, and damping matrices, respectively; $\boldsymbol{\tau}_*(t) = [\tau_{*u}(t)\ \tau_{*v}(t)\ \tau_{*r}(t)]^{\text{T}} \in \mathbb{R}^3$ is the controllable input referring to the forces $\tau_{*u}(t)$, $\tau_{*v}(t)$, and moment $\tau_{*r}(t)$ in the body-fixed frame; $\boldsymbol{\tau}_{*\text{wind}}(t) \in \mathbb{R}^3$ and $\boldsymbol{\tau}_{*\text{wave}}(t) \in \mathbb{R}^3$ are the wind and wave forces.

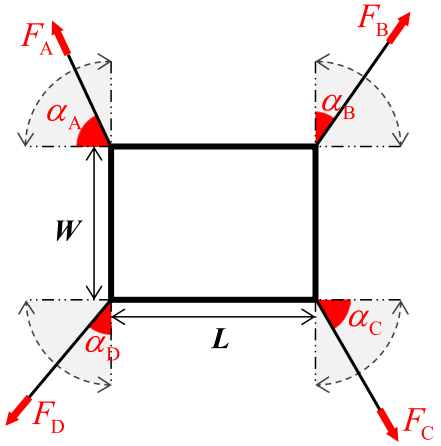

Fig. 2. Force diagram of the offshore platform.

A. Dynamics of the Offshore Platform

Fig. 2 shows the force diagram of the offshore platform. The controllable inputs denoted by $\boldsymbol{\tau}_O(t)$ are the forces from the towing lines applied by the four tugs. These tugs are defined with two roles: Role A and B are guiding tugs, whose role is to accelerate the platform and adjust its heading; Role C and D are following tugs, whose role is to slow down the platform and stabilize its heading. Then, $\boldsymbol{\tau}_O(t)$ are expressed as

$$\begin{aligned}\boldsymbol{\tau}_O(t) = \boldsymbol{B}_{O_{\text{A}}}(\alpha_{\text{A}}(t))F_{\text{A}}(t) + \boldsymbol{B}_{O_{\text{B}}}(\alpha_{\text{B}}(t))F_{\text{B}}(t)\\ + \boldsymbol{B}_{O_{\text{C}}}(\alpha_{\text{C}}(t))F_{\text{C}}(t) + \boldsymbol{B}_{O_{\text{D}}}(\alpha_{\text{D}}(t))F_{\text{D}}(t)\end{aligned} \tag{3}$$

where $F_{\text{A}}(t) \sim F_{\text{D}}(t)$ are the towing forces, and $\alpha_{\text{A}}(t) \sim \alpha_{\text{D}}(t)$ are the towing angles. The range of towing angle is defined clockwise from 0° to 90° (the gray areas in Fig. 2), which is to prevent collisions between tugs. The terms $\boldsymbol{B}_{O_{\text{A}}} \sim \boldsymbol{B}_{O_{\text{D}}} \in \mathbb{R}^3$

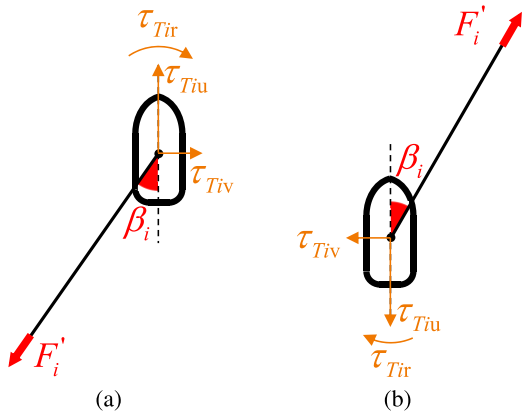

Fig. 3. Force diagram of the tugs. (a) Role A and B. (b) Role C and D.

are the platform configuration matrix, expressed as

$$\boldsymbol{B}_{O_{\mathrm{A}}} = \begin{bmatrix} \sin(\alpha_{\mathrm{A}}(t)) \\ -\cos(\alpha_{\mathrm{A}}(t)) \\ 0.5L\sin(\alpha_{\mathrm{A}}(t)) - 0.5W\cos(\alpha_{\mathrm{A}}(t)) \end{bmatrix} \tag{4}$$

$$\boldsymbol{B}_{O_{\mathrm{B}}} = \begin{bmatrix} \cos(\alpha_{\mathrm{B}}(t)) \\ \sin(\alpha_{\mathrm{B}}(t)) \\ 0.5W\sin(\alpha_{\mathrm{B}}(t)) - 0.5L\cos(\alpha_{\mathrm{B}}(t)) \end{bmatrix} \tag{5}$$

$$\boldsymbol{B}_{O_{\mathrm{C}}} = \begin{bmatrix} -\sin(\alpha_{\mathrm{C}}(t)) \\ \cos(\alpha_{\mathrm{C}}(t)) \\ 0.5L\sin(\alpha_{\mathrm{C}}(t)) - 0.5W\cos(\alpha_{\mathrm{C}}(t)) \end{bmatrix} \tag{6}$$

$$\boldsymbol{B}_{O_{\mathrm{D}}} = \begin{bmatrix} -\cos(\alpha_{\mathrm{D}}(t)) \\ -\sin(\alpha_{\mathrm{D}}(t)) \\ 0.5W\sin(\alpha_{\mathrm{D}}(t)) - 0.5L\cos(\alpha_{\mathrm{D}}(t)) \end{bmatrix} \tag{7}$$

where L and W are the length and width of the platform.

B. Dynamics of the Tugboats

Fig. 3 shows the force diagram of the tugs. The controllable inputs denoted by $\boldsymbol{\tau}_I(t)$ are the resultant forces by the thruster forces (omnidirectional forces generated by azimuth thrusters [12]) and the towline reaction forces.

For the guiding tugs (A and B), the effects from the towline are the drag forces [as seen in Fig. 3(a)], the controllable inputs are expressed as

$$\boldsymbol{\tau}_I(t) = \boldsymbol{\tau}_{T_I}(t) - \boldsymbol{B}_T(\beta_I(t))F_I'(t), \quad (I = \mathrm{A}, \mathrm{B}) \tag{8}$$

for the following tugs (C and D), the effects from the towline are the propulsive forces [as seen in Fig. 3(b)], the controllable inputs are expressed as:

$$\boldsymbol{\tau}_I(t) = \boldsymbol{\tau}_{T_I}(t) + \boldsymbol{B}_T(\beta_I(t))F_I'(t), \quad (I = \mathrm{C}, \mathrm{D}) \tag{9}$$

where $\boldsymbol{\tau}_{T_I}(t) = [\tau_{T_{Iu}}(t)\ \tau_{T_{Iv}}(t)\ \tau_{T_{Iu}}(t)]^{\mathrm{T}} \in \mathbb{R}^3$ is the thruster forces of the tug I; $F_I'(t)$ is the force applied through a controlled winch onboard the tugboat to the towing line. Assuming no force loss on the towing line, then $F_I'(t) \equiv F_I(t)$. The winch onboard can control the length of the towline to ensure it is tight. Since the scope of this work focuses on the high-level control, the low-level winch control is not considered. The term $\boldsymbol{B}_T \in \mathbb{R}^3$ is the tug configuration matrix, which is a function of the tug angle $\beta_I(t)$

$$\boldsymbol{B}_T = \begin{bmatrix} \cos(\beta_I(t)) \\ \sin(\beta_I(t)) \\ 0 \end{bmatrix}, \quad (I = \mathrm{A}, \mathrm{B}, \mathrm{C}, \mathrm{D}). \tag{10}$$

C. Effects of the Environmental Disturbances

The effects of wind disturbances on a vessel can be expressed by [23]

$$\boldsymbol{\tau}_{*\mathrm{wind}}(t) = \frac{1}{2}\rho_a V_{\mathrm{rw}}^2(t) \begin{bmatrix} -c_x\cos(\gamma_{\mathrm{rw}}(t))A_{\mathrm{Fw}} \\ c_y\sin(\gamma_{\mathrm{rw}}(t))A_{\mathrm{Lw}} \\ c_n\sin(2\gamma_{\mathrm{rw}}(t))A_{\mathrm{Lw}}L_{\mathrm{oa}} \end{bmatrix} \tag{11}$$

where ρ_a is the air density; c_x, c_y, and c_n are the wind coefficients for horizontal plane motions; A_{Fw} and A_{Lw} are the transverse and lateral projected areas of the vessel above the water, respectively; L_{oa} is the overall length of vessel; $V_{\mathrm{rw}}(t)$ and $\gamma_{\mathrm{rw}}(t)$ are the relative wind speed and the wind angle of attack relative to the vessel bow, respectively.

The effects of wave disturbances on a vessel can be modeled by simplifying the wave excitation forces [13], [24], [25]

$$\boldsymbol{\tau}_{*\mathrm{wave}}(t) = \sum_{q=1}^{N} \begin{bmatrix} K_{*qX}(t) & & \\ & K_{*qY}(t) & \\ & & K_{*qN}(t) \end{bmatrix} \cdot \begin{bmatrix} A_q\cos(\omega_q t + \varepsilon_{qX}) \\ A_q\cos(\omega_q t + \varepsilon_{qY}) \\ A_q\cos(\omega_q t + \varepsilon_{qN}) \end{bmatrix} \tag{12}$$

where q is the qth wave component; N is the total number of harmonic components; A_q is the wave amplitude; ω_q is the wave frequency; ε_{qX}, ε_{qY} and ε_{qN} are random phase angles; $K_{*qX}(t)$, $K_{*qY}(t)$, and $K_{*qN}(t)$ are the tunable gains related to the wave encounter angle $\chi_{*q}(t)$ and wave frequency ω_q [26]. To simplify the model, the tunable gains are modeled as follows:

$$\begin{aligned} K_{*qX}(t) &= k_{*qX} \cdot \cos\big(\chi_{*q}(t)\big) \\ K_{*qY}(t) &= k_{*qY} \cdot \sin\big(\chi_{*q}(t)\big) \\ K_{*qN}(t) &= k_{*qN} \cdot \sin\big(\chi_{*q}(t)\big) \\ \chi_{*q}(t) &= \beta_{qw} - \psi_*(t) \end{aligned} \tag{13}$$

where k_{*qX}, k_{*qY}, and k_{*qN} are the constant gains; β_{qw} is the incident wave angle of the qth wave component.

The effects of irrotational current disturbances on a vessel reflect on the vessel kinetics (2) [23]

$$\begin{aligned} &\boldsymbol{M}_*\dot{\boldsymbol{\nu}}_{*r}(t) + \boldsymbol{C}_*(\boldsymbol{\nu}_{*r}(t))\boldsymbol{\nu}_{*r}(t) + \boldsymbol{D}_*\boldsymbol{\nu}_{*r}(t) \\ &\quad = \boldsymbol{\tau}_*(t) + \boldsymbol{\tau}_{*\mathrm{wind}}(t) + \boldsymbol{\tau}_{*\mathrm{wave}}(t) \end{aligned} \tag{14}$$

where $\boldsymbol{\nu}_{*r}(t)$ is the relative velocity, calculated by

$$\boldsymbol{\nu}_{*r}(t) = \boldsymbol{\nu}_*(t) - \boldsymbol{\nu}_c(t) \tag{15}$$

where $\boldsymbol{\nu}_c(t)$ is the current velocity in the body-fixed frame

$$\boldsymbol{\nu}_c(t) = \begin{bmatrix} u_c(t) \\ v_c(t) \\ 0 \end{bmatrix} = \begin{bmatrix} V_c\cos(\beta_c - \psi_*(t)) \\ V_c\sin(\beta_c - \psi_*(t)) \\ 0 \end{bmatrix} \tag{16}$$

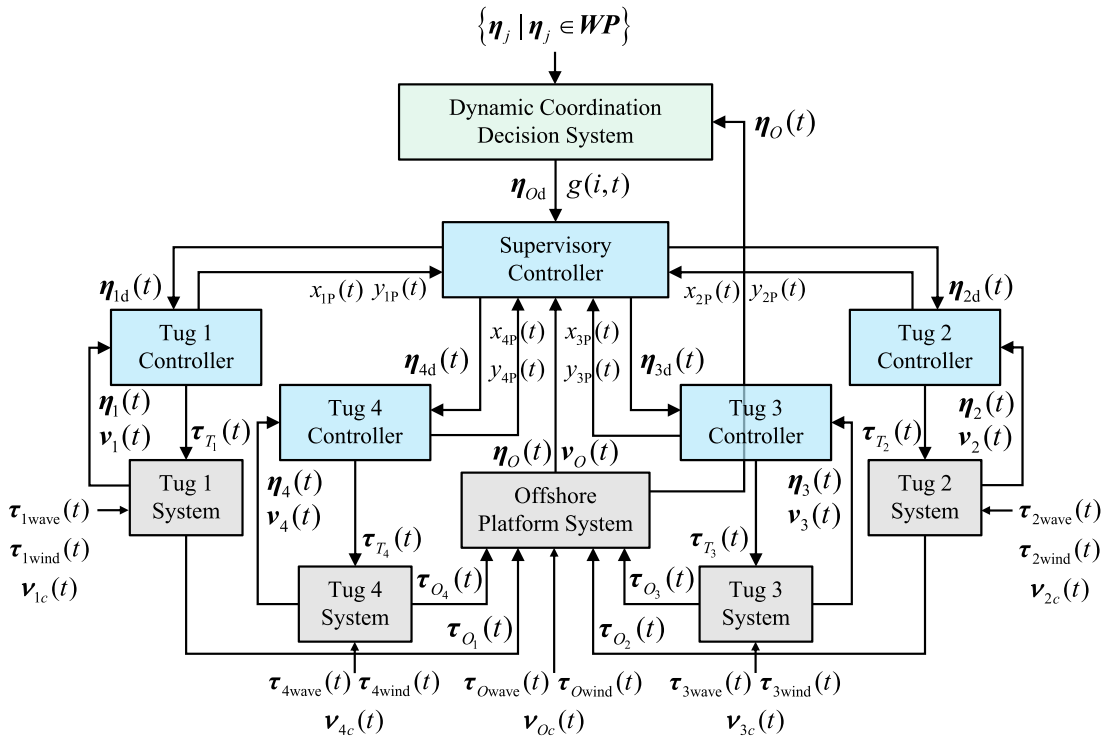

Fig. 4. Control diagram for the offshore platform towing system.

where V_c is the current speed; β_c is the sideslip angle. Thus, the derivative of $\boldsymbol{v}_{*r}(t)$ in (14) is expressed as

$$\dot{\boldsymbol{v}}_{*r}(t) = \dot{\boldsymbol{v}}_{*}(t) - \begin{bmatrix} V_c \sin(\beta_c - \psi(t)) \cdot r(t) \\ -V_c \cos(\beta_c - \psi(t)) \cdot r(t) \\ 0 \end{bmatrix}. \tag{17}$$

III. Distributed Dynamic Coordination Control

The dynamic coordination control scheme for a four-autonomous tugboat offshore platform towing system is introduced in this section.

The control diagram is shown in Fig. 4. The dynamic coordination decision system (located on the platform) outputs the desired position of the platform $\boldsymbol{\eta}_{Od}$ and the functional role of each tugboat $g(i,t), (i \in \{1,2,3,4\})$ according to the waypoint set **WP** and the current position vector of the platform $\boldsymbol{\eta}_O(t)$. The supervisory controller (located on the platform) uses the calculated $\boldsymbol{\eta}_{Od}$, $g(i,t)$, and the data of the platform $\boldsymbol{\eta}_O(t)$, $\boldsymbol{v}_O(t)$ to compute the desired position of the tugboats $\boldsymbol{\eta}_{id}(t)$. According to the information of $\boldsymbol{\eta}_{id}(t)$ and the current tug position $\boldsymbol{\eta}_i(t)$ and velocity $\boldsymbol{v}_i(t)$, the tug controller (located on the tugboat) computes the thruster forces $\boldsymbol{\tau}_{Ti}(t)$ and predicted position $[x_{iP}(t), y_{iP}(t)]$ for each tug. The data $[x_{iP}(t), y_{iP}(t)]$ are sent back to the supervisory controller to compare with the tug desired position to reach a consensus between the supervisory controller and each tug controller. When the consensus is achieved, the tug controller sends $\boldsymbol{\tau}_{Ti}(t)$ to the tug system under the environmental disturbances $\boldsymbol{\tau}_{i\text{wind}}(t)$, $\boldsymbol{\tau}_{i\text{wave}}(t)$, $\boldsymbol{v}_{ic}(t)$. Finally, each tugboat outputs the towing forces $\boldsymbol{\tau}_{O_i}(t)$ according to the system configuration to the offshore platform system under the environmental disturbances $\boldsymbol{\tau}_{O\text{wind}}(t)$, $\boldsymbol{\tau}_{O\text{wave}}(t)$, and $\boldsymbol{v}_{Oc}(t)$ for executing transportation missions.

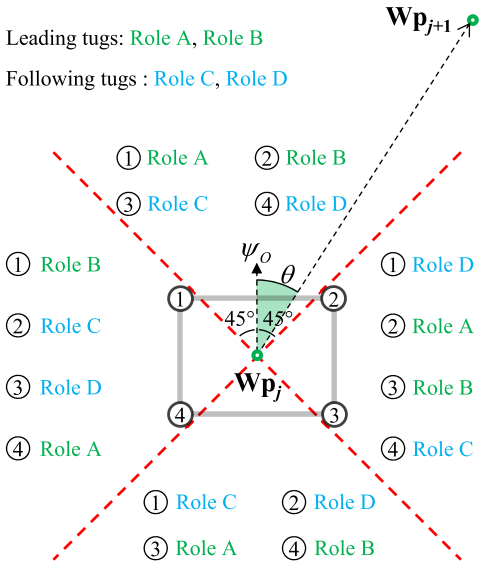

Fig. 5. Idea of the dynamic coordination.

The details of the dynamic coordination decision mechanism, the controller design, and the distributed control architecture design are introduced below.

A. Dynamic Coordination Decision Mechanism

The idea of the dynamic coordination decision is based on the relative position between the neighbor waypoints. As shown in Fig. 5, the water space around the platform

Algorithm 1 Dynamic Coordination Decision Mechanism

Calculate $\theta(t)$ according to (18);
if $-45^\circ \le \theta(t) < 45^\circ$ **then**
    Assign: role A to $g(1,t)$; role B to $g(2,t)$; role C to $g(3,t)$; role D to $g(4,t)$;
else if $45^\circ \le \theta(t) < 135^\circ$ **then**
    Assign: role B to $g(1,t)$; role C to $g(2,t)$; role D to $g(3,t)$; role A to $g(4,t)$;
else if $135^\circ \le \theta(t) < 180^\circ$ & $-180^\circ \le \theta(t) < -135^\circ$ **then**
    Assign: role C to $g(1,t)$; role D to $g(2,t)$; role A to $g(3,t)$; role B to $g(4,t)$;
else $-135^\circ \le \theta(t) < -45^\circ$
    Assign: role D to $g(1,t)$; role A to $g(2,t)$; role B to $g(3,t)$; role C to $g(4,t)$;
end if
Send $g(i,t)$ to the Control Allocation System

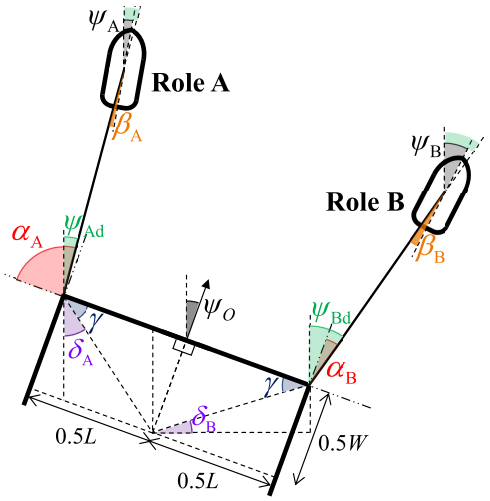

Fig. 6. Desired geometrical configuration for the front tugs.

is divided into four areas, and the angle range of each area is 90°. When the platform reaches the waypoint Wp_j and the relative position angle θ to the next waypoint Wp_{j+1} lies in a specific area, the two tugboats closer to the next waypoint are appointed as the guiding tugs (role A and B), the other two tugboats are appointed as the following tugs (role C and D). The calculation of the relative position angle is expressed as

$$\theta(t) = \arctan\left(\frac{x_{\mathrm{wp}}(j+1) - x_{\mathrm{wp}}(j)}{y_{\mathrm{wp}}(j+1) - y_{\mathrm{wp}}(j)}\right) - \psi_O(t) \tag{18}$$

where $[x_{\mathrm{wp}}(j), y_{\mathrm{wp}}(j)]$ and $[x_{\mathrm{wp}}(j+1), y_{\mathrm{wp}}(j+1)]$ are the coordinates of the waypoint Wp_j and Wp_{j+1}, respectively. Therefore, the decision mechanism of the functional role for four tugboats is provided in **Algorithm 1**.

Each role corresponds to a specific reference trajectory of the tugboat, which is calculated through the desired kinematics configuration of the towing system. For the guiding tugs A and B (as shown in Fig. 6), the key to coupling the motion of the platform and the tugboats are the following

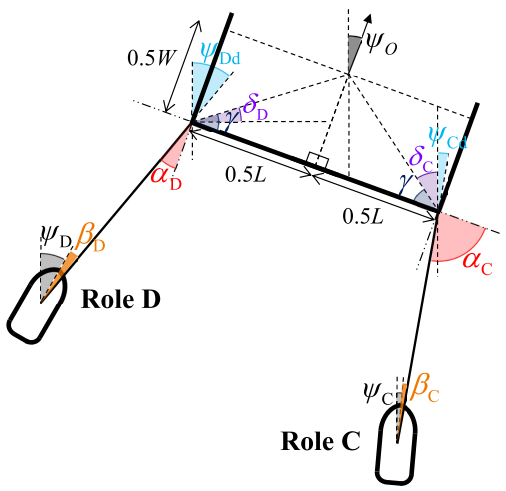

Fig. 7. Desired geometrical configuration for the rear tugs.

angles:

$$\gamma = \arctan\left(\frac{W}{L}\right)$$
$$\delta_{\mathrm{A}}(t) = 90^\circ - \gamma - \psi_O(t)$$
$$\delta_{\mathrm{B}}(t) = \gamma - \psi_O(t) \tag{19}$$

where γ is the platform configuration angle; $\delta_{\mathrm{A}}(t)$ and $\delta_{\mathrm{B}}(t)$ are the linking angles of tug A and B. The reference position and heading of the tugboats then are expressed as

$$\begin{aligned}
\psi_{\mathrm{A}d}(t) &= \alpha_{\mathrm{A}}(t) + \psi_O(t) - 90^\circ \\
x_{\mathrm{A}d}(t) &= x_O(t) + L_O\cos(\delta_{\mathrm{A}}(t)) + L_{\mathrm{tow}}\cos(\psi_{\mathrm{A}d}(t)) \\
y_{\mathrm{A}d}(t) &= y_O(t) - L_O\sin(\delta_{\mathrm{A}}(t)) + L_{\mathrm{tow}}\sin(\psi_{\mathrm{A}d}(t)) \qquad (20) \\
\psi_{\mathrm{B}d}(t) &= \alpha_{\mathrm{B}}(t) + \psi_O(t) \\
x_{\mathrm{B}d}(t) &= x_O(t) - L_O\sin(\delta_{\mathrm{B}}(t)) + L_{\mathrm{tow}}\cos(\psi_{\mathrm{B}d}(t)) \\
y_{\mathrm{B}d}(t) &= y_O(t) + L_O\cos(\delta_{\mathrm{B}}(t)) + L_{\mathrm{tow}}\sin(\psi_{\mathrm{B}d}(t)) \qquad (21)
\end{aligned}$$

where L_{tow} is the desired length of the towline (all the towlines are assumed of equal length); L_O is the distance from the center of gravity of the platform to its towing point, which is calculated by

$$L_O = \sqrt{(0.5L)^2 + (0.5W)^2}. \tag{22}$$

For the following tugs C and D (as shown in Fig. 7), the key angles are calculated by:

$$\delta_{\mathrm{C}}(t) = 90^\circ - \gamma - \psi_O(t)$$
$$\delta_{\mathrm{D}}(t) = \gamma - \psi_O(t) \tag{23}$$

where $\delta_{\mathrm{C}}(t)$ and $\delta_{\mathrm{D}}(t)$ are the linking angles of tug C and D. The reference position and heading of the tugboats then are expressed as

$$\begin{aligned}
\psi_{\mathrm{C}d}(t) &= \alpha_{\mathrm{C}}(t) + \psi_O(t) - 90^\circ \\
x_{\mathrm{C}d}(t) &= x_O(t) - L_O\cos(\delta_{\mathrm{C}}(t)) - L_{\mathrm{tow}}\cos(\psi_{\mathrm{C}d}(t)) \\
y_{\mathrm{C}d}(t) &= y_O(t) + L_O\sin(\delta_{\mathrm{C}}(t)) - L_{\mathrm{tow}}\sin(\psi_{\mathrm{C}d}(t)) \qquad (24) \\
\psi_{\mathrm{D}d}(t) &= \alpha_{\mathrm{D}}(t) + \psi_O(t) \\
x_{\mathrm{D}d}(t) &= x_O(t) + L_O\sin(\delta_{\mathrm{D}}(t)) - L_{\mathrm{tow}}\cos(\psi_{\mathrm{D}d}(t)) \\
y_{\mathrm{D}d}(t) &= y_O(t) - L_O\cos(\delta_{\mathrm{D}}(t)) - L_{\mathrm{tow}}\sin(\psi_{\mathrm{D}d}(t)). \qquad (25)
\end{aligned}$$

Besides, Figs. 6 and 7 show that the tug angle $\beta_I(t)$ in (10) can be solved by the towing angle, tugboat heading, and platform heading

$$\begin{aligned}\beta_{\mathrm{A}}(t) &= \alpha_{\mathrm{A}}(t) + \psi_O(t) - 90^\circ - \psi_{\mathrm{A}}(t)\\ \beta_{\mathrm{B}}(t) &= \alpha_{\mathrm{B}}(t) + \psi_O(t) - \psi_{\mathrm{B}}(t)\\ \beta_{\mathrm{C}}(t) &= \alpha_{\mathrm{C}}(t) + \psi_O(t) - 90^\circ - \psi_{\mathrm{C}}(t)\\ \beta_{\mathrm{D}}(t) &= \alpha_{\mathrm{D}}(t) + \psi_O(t) - \psi_{\mathrm{D}}(t).\end{aligned} \tag{26}$$

B. Controller Design

According to Fig. 4, there are two types of controllers. The supervisory controller aims to allocate the control inputs of the platform $\boldsymbol{\tau}_O(t)$ to the four tugboats by calculating the corresponding towing angles and forces. The tug controller calculates the thrust forces and moment for the tugboats $\boldsymbol{\tau}_i(t)$ to provide the towing forces and track the tug's reference trajectories. Since an offshore platform transportation towing system is characterized by multiple control inputs, has multiple control constraints, and is often highly heterogeneous, the MPC method is used to achieve control allocation and trajectory tracking.

For the offshore platform, the MPC-based supervisory controller is to solve the following optimization problem:

$$\begin{aligned}&\min_{\boldsymbol{\tau}_O} \sum_{h=1}^{H_P} J_O(k+h|k)\\ &\text{s.t. i) Platform dynamics}\\ &\quad\text{ii) Actuator saturation}\\ &\quad\text{iii) System configuration restriction}\end{aligned} \tag{27}$$

where H_P is the length of the prediction horizon; k is the current time instant; h is the hth time prediction step; $J_O(k+h|k)$ are the prediction made at k about the cost function of the ship at $k+h$.

The control objectives of the offshore platform are to track the waypoints and steady the heading, so the cost function at time instant k is designed as

$$\begin{aligned}J_O(k) = {}& w_P \boldsymbol{e}_P^{\mathrm{T}}(k)\boldsymbol{e}_P(k) + w_H \psi_{Op}^2(k)\\ &+ w_V \boldsymbol{v}_{Op}^{\mathrm{T}}(k)\boldsymbol{v}_{Op}(k)\end{aligned} \tag{28}$$

where w_P, w_H, and w_V are the weight coefficients of the platform (positive scalar); $\boldsymbol{e}_P(k) \in \mathbb{R}^2$ is the position error expressed as

$$\boldsymbol{e}_P(k) = \begin{bmatrix} x_{Op}(k) & y_{Op}(k)\end{bmatrix}^{\mathrm{T}} - \begin{bmatrix} x_{\mathrm{wp}}(j) & y_{\mathrm{wp}}(j)\end{bmatrix}^{\mathrm{T}} \tag{29}$$

where $x_{Op}(k)$, $y_{Op}(k)$ are the predicted position coordinates; $\psi_{Op}(k)$ is the predicted heading; $\boldsymbol{v}_{Op}(k) \in \mathbb{R}^3$ is the predicted velocity vector.

The predicted states $\boldsymbol{v}_{Op}(k)$, $x_{Op}(k)$, $y_{Op}(k)$, and $\psi_{Op}(k)$ in (28) and (29) satisfy the platform dynamics (the first constraint), calculated by the discretization of (1)–(7)

$$\begin{aligned}\boldsymbol{\eta}_{O_p}(k+1) = {}& \boldsymbol{\eta}_{O_p}(k) + \int_{kT_s}^{(k+1)T_s} \boldsymbol{R}(\psi_O(t))\boldsymbol{v}_O(t)dt\\ \boldsymbol{v}_{O_p}(k+1) = {}& \boldsymbol{v}_{O_p}(k) + \int_{kT_s}^{(k+1)T_s} \boldsymbol{M}_O^{-1}\\ &\times [-\boldsymbol{C}_O(\boldsymbol{v}_O(t))\cdot \boldsymbol{v}_O(t) - \boldsymbol{D}_O(\boldsymbol{v}_O(t))\boldsymbol{v}_O(t)\\ &+ \sum_{i=1}^{4} \boldsymbol{B}_O(\alpha_i(t))F_i(t) + \boldsymbol{\tau}_{O\mathrm{wind}}(t)\\ &+ \boldsymbol{\tau}_{O\mathrm{wave}}(t)]dt\end{aligned} \tag{30}$$

where T_s is the sample time.

The actuator saturation (the second constraint) stemming from the physical laws and maritime practice [12] are (for $i \in \{1,2,3,4\}$)

$$\alpha_{i\,\min} \le \alpha_i(k) < \alpha_{i\,\max} \tag{31}$$

$$0 \le F_i(k) \le F_{i\,\max} \tag{32}$$

$$\left|\dot{\alpha}_i(k)\right| \le \bar{\alpha}_i \tag{33}$$

$$\left|\dot{F}_i(k)\right| \le \bar{F}_i \tag{34}$$

where $\alpha_{i\,\min}$ and $\alpha_{i\,\max}$ are the minimum and maximum values of the towing angle; $F_{i\,\max}$ is the maximum value of the towing force that the towline withstands; $\bar{\alpha}_i$ and $\bar{F}_i$ are the maximum rates of change for the towing angle and force, respectively.

For the ith tugboat, the MPC-based tug controller is to solve the following optimization problem:

$$\begin{aligned}&\min_{\boldsymbol{\tau}_{T_i}} \sum_{h=1}^{H_P} J_i(k+h|k)\\ &\text{s.t. i) Tugboat dynamics}\\ &\quad\text{ii) Actuator saturation}\\ &\quad\text{iii) System configuration restriction}\end{aligned} \tag{35}$$

where the cost function is designed as

$$J_i(k) = w_{\mathrm{I}} \boldsymbol{e}_i^{\mathrm{T}}(k)\boldsymbol{e}_i(k) + w_{\mathrm{II}} \boldsymbol{v}_{ip}^{\mathrm{T}}(k)\boldsymbol{v}_{ip}(k) \tag{36}$$

where w_{I} and w_{II} are the weight coefficients of the tugboat (positive scalar); $\boldsymbol{v}_{ip}(k) \in \mathbb{R}^3$ is the predicted velocity vector; $\boldsymbol{e}_i(k) \in \mathbb{R}^3$ is the position and heading error of the tugboat i, expressed as

$$\boldsymbol{e}_i(k) = \boldsymbol{\eta}_{ip}(k) - \boldsymbol{\eta}_{id}(k) \tag{37}$$

where $\boldsymbol{\eta}_{ip}(k) \in \mathbb{R}^3$ and $\boldsymbol{\eta}_{id}(k) \in \mathbb{R}^3$ are the predicted and desired trajectory of the tugboat i, respectively.

The predicted states $\boldsymbol{v}_{ip}(k)$, $\boldsymbol{\eta}_{ip}(k)$ in (36) and (37) satisfy the tugboat dynamics (the first constraint), calculated by the discretization of (1) and (2) and (8)–(10)

$$\begin{aligned}\boldsymbol{\eta}_{i_p}(k+1) = {}& \boldsymbol{\eta}_{i_p}(k) + \int_{kT_s}^{(k+1)T_s} \boldsymbol{R}(\psi_i(t))\boldsymbol{v}_i(t)dt\\ \boldsymbol{v}_{i_p}(k+1) = {}& \boldsymbol{v}_{i_p}(k) + \int_{kT_s}^{(k+1)T_s} \boldsymbol{M}_i^{-1}\\ &\times [-\boldsymbol{C}_i(\boldsymbol{v}_i(t))\cdot \boldsymbol{v}_i(t) - \boldsymbol{D}_i(\boldsymbol{v}_i(t))\boldsymbol{v}_i(t)\\ &+ \boldsymbol{B}_i(\beta_i(t))F_i'(t) + \boldsymbol{\tau}_{T_i}(t)\\ &+ \boldsymbol{\tau}_{i\mathrm{wind}}(t) + \boldsymbol{\tau}_{i\mathrm{wave}}(t)]dt.\end{aligned} \tag{38}$$

The tug actuator saturation is expressed as

$$-\boldsymbol{\tau}_{Ti\,\max} \le \boldsymbol{\tau}_{Ti}(k) \le \boldsymbol{\tau}_{Ti\,\max} \tag{39}$$

$$\left|\dot{\boldsymbol{\tau}}_{Ti}(k)\right| \le \bar{\boldsymbol{\tau}}_{Ti} \tag{40}$$

where $\boldsymbol{\tau}_{i\,\max}$ and $\bar{\boldsymbol{\tau}}_{Ti}$ are the maximum value and maximum change rate of the thruster forces and moment, respectively.

The system configuration restriction (the third constraint) in (27) and (35) are used to reach a consensus between the supervisory controller and the tug controllers for achieving the distributed control architecture, illustrated in Section III-C.

C. Distributed Control Architecture Design

The distributed control architecture is achieved using the alternating direction method of multipliers (ADMM) [27]. In our case, the key to reaching a consensus between the supervisory controller and the tug controllers is to make the difference between the desired tug trajectory $[\boldsymbol{\eta}_{id}(k)]$ and the predicted tug trajectory $[\boldsymbol{\eta}_{ip}(k)]$ as small as possible.

Under the assumption of no delay and package loss of communication between each system, the desired tug trajectory $\boldsymbol{\eta}_{id}(k)$ is calculated through (19)–(25). However, (26) indicates that the desired tug heading will not be achieved immediately by the tug controller, especially in the process of functional role changing. Thus, to make the switching process between the tug role of guiding and following smooth, the desired tug position is the key element for reaching a consensus other than the desired tug heading. Then, the tugboat cost function except for the position consensus part is revised from (36) to

$$J_{Ti}(k) = w_{\mathrm{IH}} e_{\psi i}^2(k) + w_{\mathrm{II}} \boldsymbol{v}_{ip}^{\mathrm{T}}(k) \boldsymbol{v}_{ip}(k) \tag{41}$$

where w_{IH} is the weight coefficient for the tugboat heading (positive scalar); $e_{\psi i}$ is the heading error of the tugboat i. Then the augmented Lagrangian form of the dynamic coordination offshore platform transportation problem at time instant k is formulated as

$$\begin{aligned} L_p\big(\boldsymbol{\tau}_O(k), \boldsymbol{\tau}_{T_i}(k), \lambda_i(k)\big) &= J_O(\boldsymbol{\tau}_O(k)) \\ &+ \sum_{i=1}^{4}\Big(J_{Ti}\big(\boldsymbol{\tau}_{T_i}(k)\big) + \lambda_i^{\mathrm{T}}(k)\big[\boldsymbol{p}_{ip}(k) - \boldsymbol{p}_{id}(k)\big] \\ &\quad + (\rho_i/2)\big\|\boldsymbol{p}_{ip}(k) - \boldsymbol{p}_{id}(k)\big\|_2^2\Big) \end{aligned} \tag{42}$$

where $\lambda_i(k)$ is the Lagrangian multiplier or dual variable, and ρ_i is the penalty parameter; $\boldsymbol{p}_{ip}(k) = [x_{ip}(k) \quad y_{ip}(k)]^{\mathrm{T}}$ and $\boldsymbol{p}_{id}(k) = [x_{id}(k) \quad y_{id}(k)]^{\mathrm{T}}$ are the predicted and desired tug positions, respectively. According to (19)–(21), $\boldsymbol{p}_{id}(k)$ is a function of the towing angle $\alpha_i(k)$ and the predicted platform position vector $\boldsymbol{\eta}_{O_P}(k)$; $\alpha_i(k)$ is a part of $\boldsymbol{\tau}_O(k)$, $\boldsymbol{\eta}_{O_P}(k)$ can be calculated by $\boldsymbol{\tau}_O(k)$ through the platform dynamics. Thus, $\boldsymbol{p}_{id}(k)$ can be expressed as a function of $\boldsymbol{\tau}_O(k)$: $\boldsymbol{p}_{id}(k) = f_i(\boldsymbol{\tau}_O(k))$. Similarly, $\boldsymbol{p}_{ip}(k)$ can be calculated by $\boldsymbol{\tau}_{T_i}(k)$ through the tug dynamics, so $\boldsymbol{p}_{ip}(k) = h_i(\boldsymbol{\tau}_{T_i}(k))$.

Therefore, the iteration procedure of the ADMM at time instant k is then formulated as follows:

$$\begin{aligned} \boldsymbol{\tau}_{T_i}^s(k) := \arg\min_{\boldsymbol{\tau}_{T_i}(k)}\Big(&J_{Ti}\big(\boldsymbol{\tau}_{T_i}(k)\big) + \lambda_i^{s-1}(k)^{\mathrm{T}} \\ &\times \big[h_i\big(\boldsymbol{\tau}_{T_i}(k)\big) - f_i\big(\boldsymbol{\tau}_O^{s-1}(k)\big)\big] + (\rho_i/2) \\ &\times \big\|h_i\big(\boldsymbol{\tau}_{T_i}(k)\big) - f_i\big(\boldsymbol{\tau}_O^{s-1}(k)\big)\big\|_2^2\Big) \end{aligned} \tag{43}$$

$$\begin{aligned} \boldsymbol{\tau}_O^s(k) := \arg\min_{\boldsymbol{\tau}_O(k)}\Big(&J_O(\boldsymbol{\tau}_O(k)) \\ &+ \sum_{i=1}^{4}\Big(-\lambda_i^{s-1}(k)^{\mathrm{T}} f_i(\boldsymbol{\tau}_O(k)) + (\rho_i/2) \\ &\times \big\|h_i\big(\boldsymbol{\tau}_{T_i}^s(k)\big) - f_i(\boldsymbol{\tau}_O(k))\big\|_2^2\Big)\Big) \end{aligned} \tag{44}$$

$$\lambda_i^s(k) := \lambda_i^{s-1}(k) + \rho_i\big(h_i\big(\boldsymbol{\tau}_{T_i}^s(k)\big) - f_i\big(\boldsymbol{\tau}_O^s(k)\big)\big) \tag{45}$$

where s is the iteration index and $\cdot^s$ stands for the corresponding variable at the sth iteration.

The termination criterion is provided based on the following residuals:

$$\begin{aligned} \left\|\boldsymbol{R}_{\mathrm{pri},i}^s(k)\right\|_2 &= \left\|h_i\big(\boldsymbol{\tau}_{T_i}^s(k)\big) - f_i\big(\boldsymbol{\tau}_O^s(k)\big)\right\|_2 \le \varepsilon_{\mathrm{pri},i}^s(k) \\ \left\|\boldsymbol{R}_{\mathrm{dual},i}^s(k)\right\|_2 &= \left\|f_i\big(\boldsymbol{\tau}_O^s(k)\big) - f_i\big(\boldsymbol{\tau}_O^{s-1}(k)\big)\right\|_2 \le \varepsilon_{\mathrm{dual},i}^s(k) \end{aligned} \tag{46}$$

where $\boldsymbol{R}_{\mathrm{pri},i}^s$ and $\boldsymbol{R}_{\mathrm{dual},i}^s$ are the primal and dual residual at iteration s; $\varepsilon_{\mathrm{pri},i}^s > 0$ and $\varepsilon_{\mathrm{dual},i}^s > 0$ are the feasibility tolerances, determined by

$$\begin{aligned} \varepsilon_{\mathrm{pri},i}^s(k) &= \sqrt{n_s}\varepsilon^{\mathrm{abs}} \\ &\quad + \varepsilon^{\mathrm{rel}} \max\left\{\left\|h_i\big(\boldsymbol{\tau}_{T_i}^s(k)\big)\right\|_2, \left\|f_i\big(\boldsymbol{\tau}_O^s(k)\big)\right\|_2\right\} \\ \varepsilon_{\mathrm{dual},i}^s(k) &= \sqrt{n_s}\varepsilon^{\mathrm{abs}} + \varepsilon^{\mathrm{rel}}\left\|\lambda_i^s(k)\right\|_2 \end{aligned} \tag{47}$$

where n_s is the size of the variable $\boldsymbol{\tau}_{T_i}$; $\varepsilon^{\mathrm{abs}} > 0$ and $\varepsilon^{\mathrm{rel}} > 0$ are the absolute and relative tolerances, respectively.

The penalty parameter ρ_i is usually designed to be variable according to the comparison of the primal and dual residuals to increase the speed of convergence

$$\rho_i^s = \begin{cases} \min\{2\rho_i^{s-1}, \rho_{i\,\max}\}, & \text{if } \left\|R_{\mathrm{pri},i}^s(k)\right\|_2 > 10\left\|R_{\mathrm{dual},i}^s(k)\right\|_2 \\ \max\{\rho_i^{s-1}/2, \rho_{i\,\min}\}, & \text{if } \left\|R_{\mathrm{pri},i}^s(k)\right\|_2 < 10\left\|R_{\mathrm{dual},i}^s(k)\right\|_2 \\ \rho_i^{s-1}, & \text{otherwise} \end{cases} \tag{48}$$

where $\rho_{i\,\max}$ and $\rho_{i\,\min}$ are the maximum and minimum values of the penalty parameter, respectively.

Therefore, the distributed control scheme is summarized in **Algorithm 2**. And the overview of the entire proposed method is shown in **Algorithm 3.**

Remark 1: To analyze the stability of the closed-loop system, some conditions for quadratic stage cost and specific terminal cost would be needed in theory [28]. For example, by computing the reachable sets of a starting region to make

Algorithm 2 Consensus Iteration for Distributed Control

Input: $\boldsymbol{\eta}_O(k)$, $\boldsymbol{\nu}_O(k)$; $\boldsymbol{\eta}_i(k)$, $\boldsymbol{\nu}_i(k)$; $\boldsymbol{\eta}_{Od}$; $g(i,t)$.

Supervisory Controller receive $g(i,t)$ from the Dynamic Coordination Decision System;
for i=1 to 4 **do**
  if $g(i,t)$ is assigned as role A **then**
    $\boldsymbol{p}_{id}(k)$ in (42) is calculated using (20);
  else if $g(i,t)$ is assigned as role B **then**
    $\boldsymbol{p}_{id}(k)$ in (42) is calculated using (21);
  else if $g(i,t)$ is assigned as role C **then**
    $\boldsymbol{p}_{id}(k)$ in (42) is calculated using (24);
  else
    $\boldsymbol{p}_{id}(k)$ in (42) is calculated using (25);
  end if
end for
for $s = 1 : S$ **do** (S is the maximum iterations)
  Step 1: Calculate $\boldsymbol{\tau}^s_{T_i}(k)$ in each tug controller according to (43), and send the results to the supervisory controller.
  Step 2: Calculate $\boldsymbol{\tau}^s_O(k)$ in the supervisory controller according to (44).
  Step 3: Update $\lambda^s_i(k)$ based on the results from **Step 1** and **Step 2** according to (45) in each tug controller.
  Step 4: Update $\varepsilon^s_{\mathrm{pri},i}(k)$ and $\varepsilon^s_{\mathrm{dual},i}(k)$ according to (47), then check if $\boldsymbol{R}^s_{\mathrm{pri},i}(k)$ and $\boldsymbol{R}^s_{\mathrm{dual},i}(k)$ meet the termination criteria according to (46) in each tug controller;
  Step 5: If (46) is not satisfied, update ρ^s_i according to (48) and return to **Step 1**; otherwise, break the iteration.
end for

Output: $\boldsymbol{\tau}^s_{T_i}(k)$; $\boldsymbol{\tau}^s_O(k)$.

Algorithm 3 Distributed Dynamic Coordination Control

Initialize all the variables and parameters;
while $\|\boldsymbol{\eta}_O(k) - \boldsymbol{\eta}_{Od}\|_2 > \varepsilon$ (ε is a small positive) **do**
  Dynamic Coordination Decision System calculates $g(i,t)$ according to **Algorithm 1**;
  Supervisory Controller and each tug controller calculate $\boldsymbol{\tau}^s_{T_i}(k)$, $\boldsymbol{\tau}^s_O(k)$ according to **Algorithm 2**;
end while

all of them contained into a targeting region, and determine the minimum admissible mode-dependent dwell time, the stability of MPC can be guaranteed [29].

In the case of the increased number of constraints due to, e.g., static boundaries, the stability of the proposed method should be investigated. A possible way could transform some hard constraints into soft ones and make them part of the objective function. For instance, when considering collision avoidance, the distance constraint from obstacles can be incorporated into the objective function by reciprocal form [30].

IV. Simulation Experiment

A simulation experiment is carried out in this section to show the performance of the proposed distributed dynamic coordination control scheme applied to an offshore platform towing system of small-scale lab vessels.

TABLE II
Data of Environmental Disturbances

Wind velocity	$V_w = 0.2$ m/s
Wind direction	$0°$, from the North
Current velocity	$V_c = 0.05$ m/s
Current direction	$180°$, to the South
Number of wave component	$N = 2$
Wave frequency	$\omega_1 = 0.5$ rad/s, $\omega_2 = 0.1$ rad/s
Incident wave angle	$\beta_{1w} = 0°$, $\beta_{2w} = 0°$
Wave amplitude	$A_1 = 0.05$ m, $A_2 = 0.1$ m
Wave phase angle	$\varepsilon_{1X} = \pi/3$, $\varepsilon_{1Y} = \pi/6$, $\varepsilon_{1N} = \pi/9$; $\varepsilon_{2X} = \pi/4$, $\varepsilon_{2Y} = \pi/8$, $\varepsilon_{2N} = \pi/12$
Wave constant gains[1]	$k_{S1X} = 0.1$, $k_{S1Y} = 0.1$, $k_{S1N} = 0$; $k_{T1X} = 0.02$, $k_{T1Y} = 0.02$, $k_{T1N} = 0$; $k_{S2X} = 0.25$, $k_{S2Y} = 0.25$, $k_{S2N} = 0$; $k_{T2X} = 0.05$, $k_{T2Y} = 0.05$, $k_{T2N} = 0$

[1] The values of the wave constant gains are related to the force Response Amplitude Operator (RAO) [23], and different dimensions of the marine craft have different gains. Since the dimension of the platform is much larger than tugboats, the value of the platform gains k_{Sq} is much larger than that of the tugboats k_{Tq} for the qth wave component.

A. Simulation Setup

The models of the simulated offshore platform and tugboat are based on the design parameters and characteristics (i.e., hydrodynamic terms) in [31] and [32]. The weight and size of the platform are $m_O = 3.345$ kg, $W = 1.2$ m, and $L = 1.6$ m; and the weight and size of the tugboat are $m_i = 16.9$ kg, $w_i = 0.2$ m, and $l_i = 0.6$ m, respectively. For the control inputs of the platform, $L_{\mathrm{tow}} = 1.5$ m, $F_{i\,\max} = 0.3$ N, and $\bar{\alpha}_i = 5°/\mathrm{s}$, $\bar{F}_i = 0.01$ N/s; for the control inputs of each tugboat, $\boldsymbol{\tau}_{i\,\max} = [2\ \mathrm{N}\ \ 2\ \mathrm{N}\ \ 1\ \mathrm{Nm}]^{\mathrm{T}}$ and $\bar{\boldsymbol{\tau}}_i = [1\ \mathrm{N/s}\ \ 1\ \mathrm{N/s}\ \ 0.5\ \mathrm{Nm/s}]^{\mathrm{T}}$.

The environmental disturbances are set as shown in Table II, consisting of winds, waves, and currents, where the effects of the waves are coupled by two wave components. The information on the control system is shown in Table III, including the parameters of the ADMM strategy. The value of weights is chosen based on the magnitude of position, heading, and velocity part in different controllers; the larger the magnitude, the smaller the weight.

Two simulation scenarios are defined with the same towing system parameters, environmental disturbances parameters, control system parameters, and control objectives, except for the mechanism of the functional role for tugboats: the tugboats

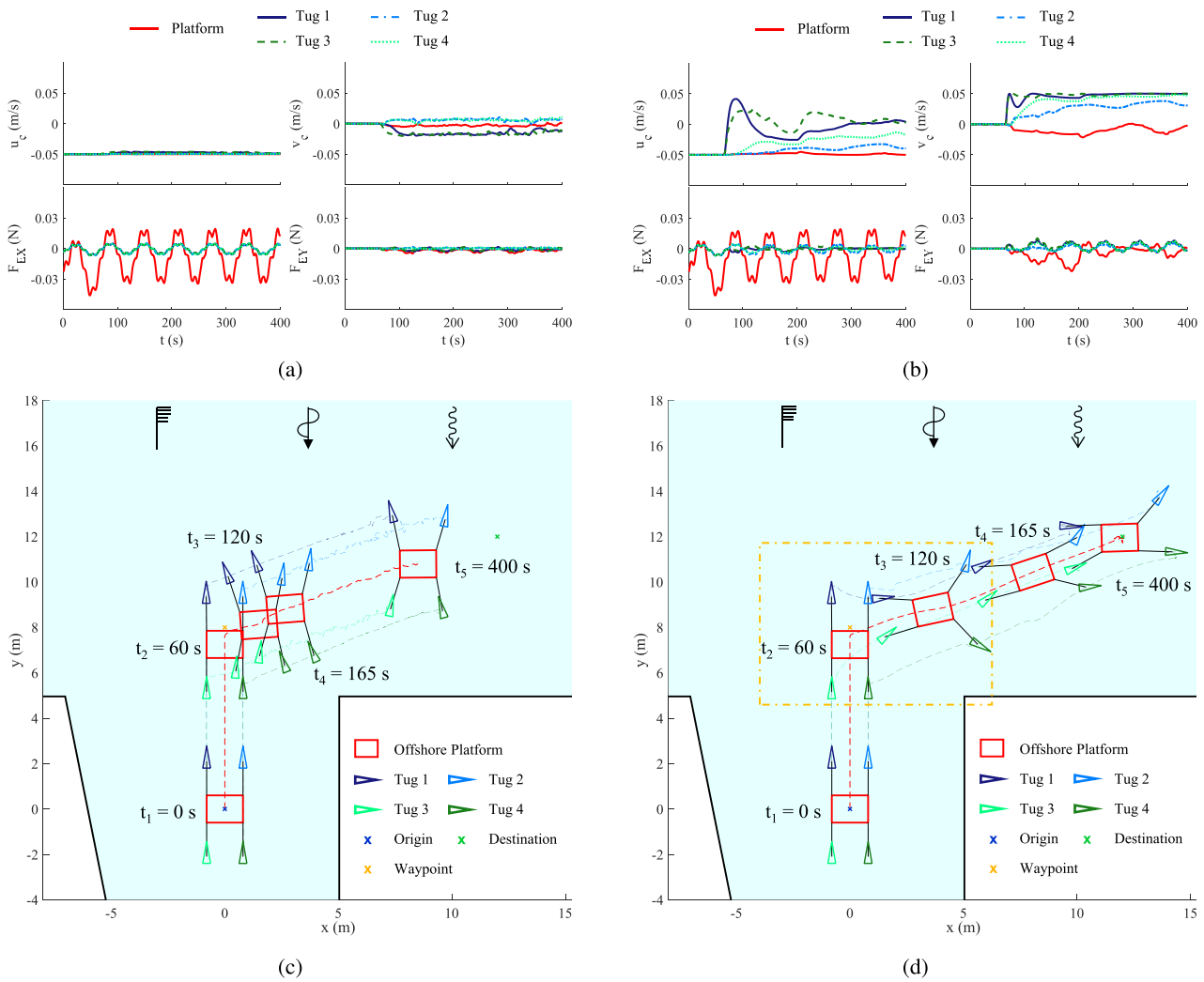

Fig. 8. Towing processes under environmental disturbances in two scenarios. (a) Current velocities (u_c, v_c) and wind and wave-resultant forces (F_{EX}, F_{EY}) on x- and y-axis in the body-fixed frame of Scenario I. (b) Current velocities (u_c, v_c) and wind and wave-resultant forces (F_{EX}, F_{EY}) on x- and y-axis in the body-fixed frame of Scenario II. (c) Towing process in Scenario I. (d) Towing process in Scenario II.

TABLE III
PARAMETERS OF THE CONTROL SYSTEM

Sample time	$T_s = 1\mathrm{s}$
Prediction horizon	$H_P = 3$
Weight coefficients of J_O	$w_{\mathrm{P}} = 1$, $w_{\mathrm{H}} = 100$, $w_{\mathrm{V}} = 20$
Weight coefficient of J_{Ti}	$w_{\mathrm{IH}} = 0.25$, $w_{\mathrm{II}} = 2$
Absolute tolerance	$\varepsilon^{\mathrm{abs}} = 0.001$
Relative tolerance	$\varepsilon^{\mathrm{rel}} = 0.001$
Minimum penalty parameter	$\rho_{i\,\min} = 1$
Maximum penalty parameter	$\rho_{i\,\max} = 100$

in Scenario I have fixed functional roles, while in Scenario II the tugboats are controlled by the proposed dynamic coordination control scheme. Simulation experiments are carried out using MATLAB 2018b on a laptop computer with an Intel CORE i7 CPU and 8 GB of RAM.

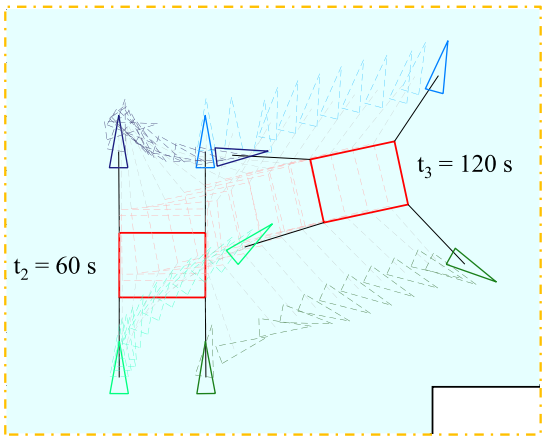

Fig. 9. Process of the functional role changes for the tugs.

B. Results and Discussion

Fig. 8 shows the towing process under environmental disturbances, where Fig. 8(a) and (b) are the effects of the winds, waves, and currents in two scenarios; Fig. 8(c) and (d) are

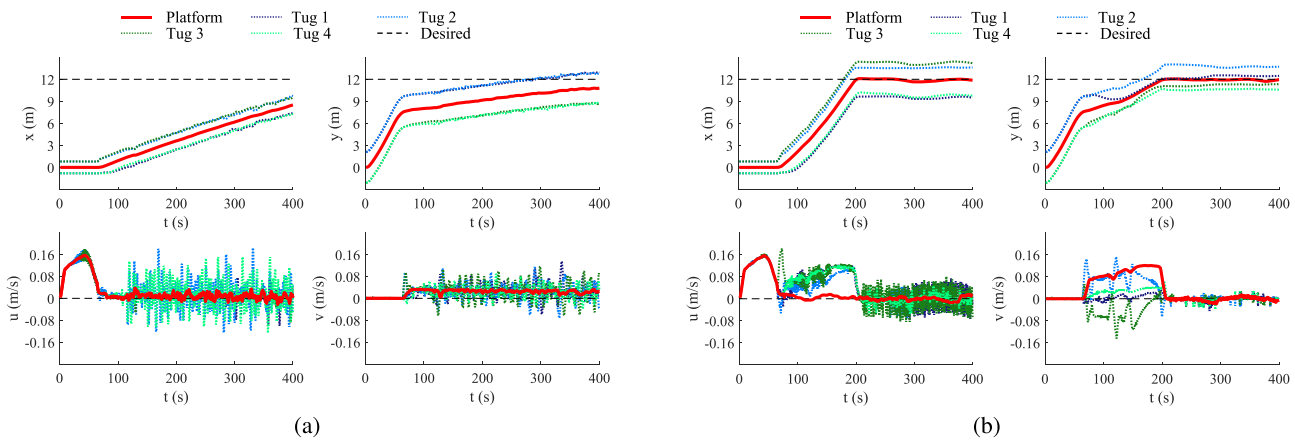

Fig. 10. Temporal evolution of the position and linear velocity of the platform and four tugs. (a) Scenario I. (b) Scenario II.

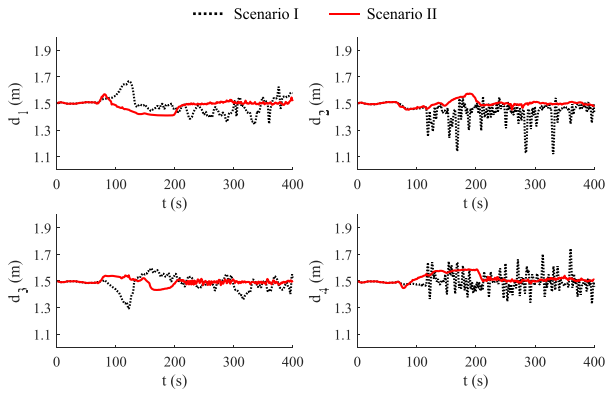

Fig. 11. Temporal evolution of the towline elongation.

TABLE IV
CONTROL PERFORMANCE OF THE TWO SCENARIOS

Scenario	Settling Time	Towline Elongation Error
I	> 400 s	$e_{l1} = 11.21\%$, $e_{l2} = 25.32\%$, $e_{l3} = 13.94\%$, $e_{l4} = 16.42\%$
II	212 s	$e_{l1} = 5.99\%$, $e_{l2} = 5.01\%$, $e_{l3} = 4.50\%$, $e_{l4} = 5.83\%$

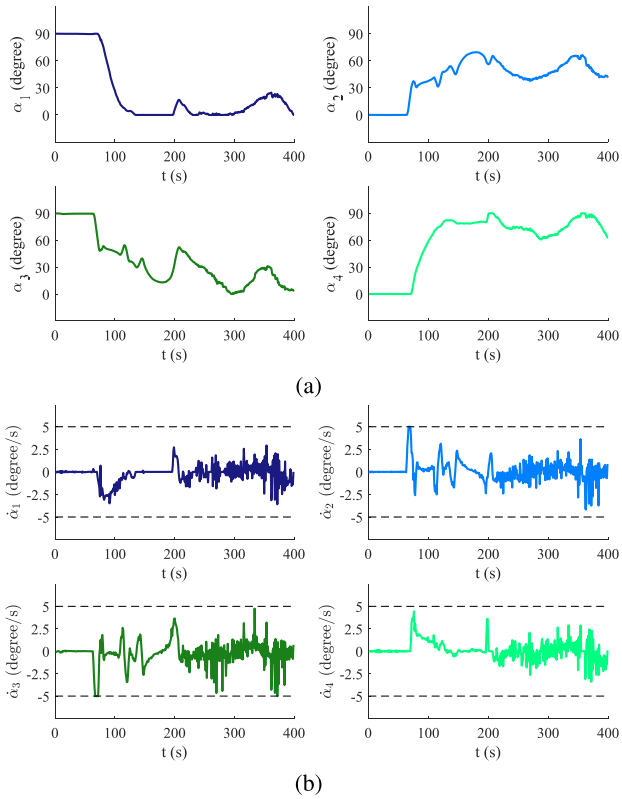

Fig. 12. Temporal evolution of the towing angles and their change rates in Scenario II. (a) Value of the four towing angles. (b) Change rate of the four towing angles.

the five time-sampled typical states of the towing system in two scenarios. From $t_1 = 0$ s to $t_2 = 60$ s, the trajectories of the platform and four tugs in two scenarios are the same (straight path), also affected by the same environmental disturbances.

From $t_2 = 60$ s to $t_3 = 120$ s the target waypoint changes, the four tugboats keep their previous configurations and slowly move the platform in Scenario I; while in Scenario II, tug 1 changes its role from guiding tug to the following tug, tug 3 changes its role from following tug to guiding tug, meanwhile the four tugboats coordinately adjust the platform toward to the destination. The process of the functional role changes for the tugs is shown in Fig. 9.

From $t_3 = 120$ s to $t_4 = 165$ s, the four tugboats in Scenario I still slowly move the platform with the same configurations. In Scenario II, tug 2 and tug 3 as the guiding tugs continue adjusting to make an all-out effort toward to the destination. Finally, from $t_4 = 165$ s to $t_5 = 400$ s, the platform in Scenario II has been transported to the destination when the same mission in Scenario I is not finished yet.

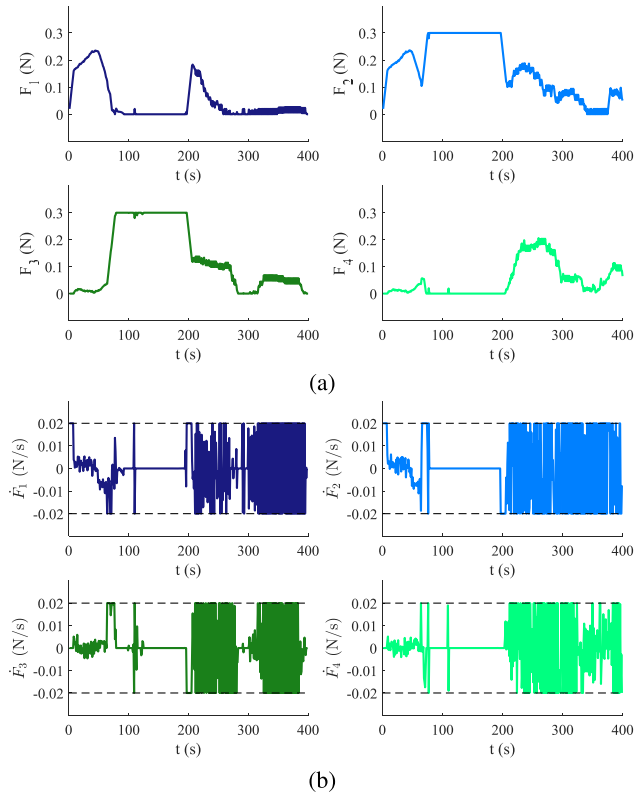

Fig. 13. Temporal evolution of the towing forces and their change rates in Scenario II. (a) Value of the four towing forces (b) Change rate of the four towing forces.

After $t_2 = 60$ s, the effects of environmental disturbances in the two scenarios are also different. For the platform, since its heading undergoes few changes in Scenario I, the environmental effects mainly work on the x-axis direction in the body-fixed frame. The platform heading in Scenario II undergoes more changes, therefore, there are environmental effects on the y-axis direction as well. The differences are more explicitly reflected in the four tugs whose environmental influence in Scenario II varies more than in Scenario I because of the functional role adjustment.

The time-varying position and linear velocity of the platform and four tugs are shown in Fig. 10. It can be seen that around 200 s, the position of the platform in Scenario II has already achieved the desired value, while the platform in Scenario I has not reached the destination yet even at the 400 s. The value of surge velocity of the platform in both scenarios has a similar variation, but for the tugs, except for the phase of the functional role adjustment, the magnitude of the surge velocity changes in Scenario II is smaller than Scenario I. The sway velocities of the platform and tugs are quite different between the two scenarios. Due to the functional role adjustment, there are great sway motions for tugs, which makes the sway velocity of the platform have a large increase after $t_2 = 60$ s. This explains the reason for the more efficiency of the towing process in Scenario II.

Fig. 11 shows the time-varying values of the towline elongation. Compared to Scenario I, the changes of the

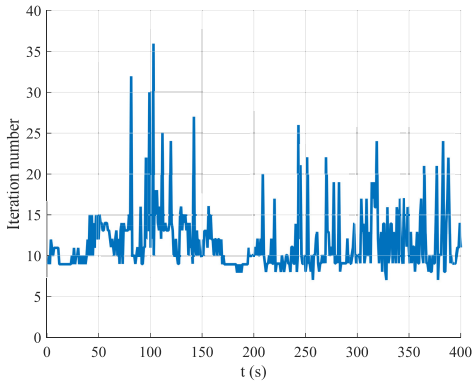

Fig. 14. Temporal evolution iteration number for consensus in Scenario II.

towline elongation in Scenario II are smaller, reflecting a better consensus achievement between the supervisory and tug controller in Scenario II. The control performance of the two scenarios, characterized by settling time and maximum towline elongation error, is quantified and compared in Table IV. The settling time is defined by the states of the ship that satisfy the following conditions: 1) the distance from the current position to the desired position is less than half length of the ship and 2) the surge and sway velocities are less than 0.01 m/s. The towline elongation error is calculated by

$$e_{\text{li}} = \left| \frac{\max\{d_i(t)\} - l_{\text{tow}}}{l_{\text{tow}}} \right|. \tag{49}$$

From Table IV, it is clear that the control performance in Scenario II is better.

The time-varying of the towing angles, towing forces, and their change rate in Scenario II are shown in Figs. 12 and 13. From Fig. 12, the four towing angels and their change rates satisfy the saturation constraints. Because of the tugboat role adjustment, the magnitude of the towing angle change is huge. From Fig. 13, during the time between 0 and 60 s, since tugs 1 and 2 are the guiding tugs and tugs 3 and 4 are the following tugs, the values of F_1 and F_2 keep increasing and F_3 and F_4 remain around zero; during the time of 60–200 s, the tugboat role adjustment makes tugs 2 and 3 guiding tugs and tugs 1 and 4 following tugs, so the values of F_1 and F_4 reduce to zero and F_3 and F_4 increase to their maximum value. After 200 s, because environmental disturbances do not vanish, the towing forces always exists against environmental forces to reach a dynamic balance for the towing system.

Regarding the total computational time cost of solving the optimization control problem, the cost in Scenario I is 3.7 times the cost in Scenario II. Considering the energy consumption, which is calculated based on the admiralty coefficient [33], the consumption in Scenario I is 0.89 times the consumption in Scenario II. The above data indicate that, a small sacrifice of energy in Scenario II can relieve the computational load. The iteration number for consensus in each time step of Scenario II is shown in Fig. 14. It is observed that the majority of numbers are under 20, and the maximum number is less than 40.

V. Conclusion and Future Research

This article proposes a distributed dynamic coordination control scheme for a multivessel towing system to transport an offshore platform under environmental disturbances. The cores of the proposed control scheme are the dynamic coordination decision mechanism, the controller design, and the distributed control architecture design.

The decision mechanism is based on the relative position between the last and the current waypoints, and four sets of functional role combinations are presented to assign the role of each tugboat. The controllers are designed based on the MPC strategy with different cost functions: for the supervisory controller, the cost function consists of the position error, heading, and velocities; for the tug controller, its cost function components are the position error, heading error, and velocities. The distributed control architecture is built based on the ADMM strategy which is to design an augmented Lagrangian function for reaching a consensus between the desired tug position output from the supervisory controller and the predicted tug position output from the tug controller. The comparison of the two Scenarios indicates that the proposed control scheme has better consensus achievement for the distributed control architecture accomplishment and more efficiently transports an offshore platform under environmental disturbances.

Future research will focus on collision avoidance for the offshore platform towing system to improve its safety when dealing with static obstacles and other moving vessels. The analysis of the stability of the proposed algorithm will be included as well. In the stability analysis, we will consider the impact of the increased number of constraints due to, e.g., static boundaries or collision avoidance regulations.

References

[1] M. Melikoglu, "Current status and future of ocean energy sources: A global review," *Ocean Eng.*, vol. 148, pp. 563–573, Jan. 2018.

[2] T. Haug et al., "Future harvest of living resources in the Arctic Ocean north of the Nordic and Barents seas: A review of possibilities and constraints," *Fisheries Res.*, vol. 188, pp. 38–57, Apr. 2017.

[3] B. C. McLellan, "Sustainability assessment of deep ocean resources," *Proc. Environ. Sci.*, vol. 28, pp. 502–508, Jan. 2015.

[4] B. J. Leira, "Multi-purpose offshore-platforms: Past, present and future research and developments," in *Proc. 36th Int. Conf. Ocean, Offshore Arctic Eng.*, Trondheim, Norway, Jun. 2017, pp. 1–11.

[5] Z. Du, V. Reppa, and R. R. Negenborn, "Cooperative control of autonomous tugs for ship towing," *IFAC-PapersOnLine*, vol. 53, no. 2, pp. 14470–14475, 2020.

[6] M. G. Feemster and J. M. Esposito, "Comprehensive framework for tracking control and thrust allocation for a highly overactuated autonomous surface vessel," *J. Field Robot.*, vol. 28, no. 1, pp. 80–100, Jan. 2011.

[7] B. Bidikli, E. Tatlicioglu, and E. Zergeroglu, "Robust dynamic positioning of surface vessels via multiple unidirectional tugboats," *Ocean Eng.*, vol. 113, pp. 237–245, Feb. 2016.

[8] V. P. Bui, H. Kawai, Y. B. Kim, and K. S. Lee, "A ship berthing system design with four tug boats," *J. Mech. Sci. Technol.*, vol. 25, no. 5, pp. 1257–1264, May 2011.

[9] S.-M. Lee, J. H. Lee, M.-I. Roh, K.-S. Kim, S.-H. Ham, and H.-W. Lee, "An optimization model of tugboat operation for conveying a large surface vessel," *J. Comput. Design Eng.*, vol. 8, no. 2, pp. 654–675, Apr. 2021.

[10] L. Chen, H. Hopman, and R. R. Negenborn, "Distributed model predictive control for cooperative floating object transport with multi-vessel systems," *Ocean Eng.*, vol. 191, Nov. 2019, Art. no. 106515.

[11] R. V. C. Rosario, J. P. V. S. Cunha, and P. B. Garcia-Rosa, "Stabilizing control of an unmanned surface vehicle pushing a floating load," *Int. J. Control, Autom. Syst.*, vol. 18, no. 12, pp. 3194–3203, Dec. 2020.

[12] H. Hensen, *Tug Use in Port: A Practical Guide*. London, U.K.: Nautical Institute, 2003.

[13] M. M. Ismail, N. G. Chalhoub, and V. Pilipchuk, "Dynamics and control of a two-ship ensemble connected by a massless towline," *Ocean Eng.*, vol. 234, Aug. 2021, Art. no. 109295.

[14] Y. Zheng, J. Tao, Q. Sun, H. Sun, M. Sun, and Z. Chen, "An intelligent course keeping active disturbance rejection controller based on double deep Q-network for towing system of unpowered cylindrical drilling platform," *Int. J. Robust Nonlinear Control*, vol. 31, no. 17, pp. 8463–8480, Aug. 2021.

[15] J. Tao, L. Du, M. Dehmer, Y. Wen, G. Xie, and Q. Zhou, "Path following control for towing system of cylindrical drilling platform in presence of disturbances and uncertainties," *ISA Trans.*, vol. 95, pp. 185–193, Dec. 2019.

[16] H. Hajieghrary, D. Kularatne, and M. A. Hsieh, "Differential geometric approach to trajectory planning: Cooperative transport by a team of autonomous marine vehicles," in *Proc. Annu. Amer. Control Conf. (ACC)*, Milwaukee, WI, USA, Jun. 2018, pp. 858–863.

[17] Z. Du, R. R. Negenborn, and V. Reppa, "Multi-vessel cooperative speed regulation for ship manipulation in towing scenarios," in *Proc. 13th IFAC Conf. Control Appl. Mar. Syst., Robot., Vehicles*, Oldenburg, Germany, 2021, pp. 1–6.

[18] Z. Du, R. R. Negenborn, and V. Reppa, "Cooperative multi-agent control for autonomous ship towing under environmental disturbances," *IEEE/CAA J. Autom. Sinica*, vol. 8, no. 8, pp. 1365–1379, Aug. 2021.

[19] A. S. S. Ianagui and E. A. Tannuri, "Automatic load maneuvering and hold-back with multiple coordinated DP vessels," *Ocean Eng.*, vol. 178, pp. 357–374, Apr. 2019.

[20] G. Xia, C. Sun, B. Zhao, X. Sun, and X. Xia, "Robust cooperative trajectory tracking control for an unactuated floating object with multiple vessels system," *ISA Trans.*, vol. 123, pp. 263–271, Apr. 2021.

[21] R. R. Negenborn and J. M. Maestre, "On 35 approaches for distributed MPC made easy," in *Distributed Model Predictive Control Made Easy* (Intelligent Systems, Control and Automation: Science and Engineering). Dordrecht, The Netherlands: Springer, 2013, pp. 1–37.

[22] Z. Du, R. R. Negenborn, and V. Reppa, "Dynamic coordination of multiple vessels for offshore platform transportation," in *Proc. IEEE Conf. Control Technol. Appl. (CCTA)*, Trieste, Italy, Aug. 2022, pp. 76–81.

[23] T. I. Fossen, *Handbook of Marine Craft Hydrodynamics and Motion Control*. Chichester, U.K.: Wiley, 2011.

[24] T. Perez, *Ship Motion Control: Course Keeping and Roll Stabilisation Using Rudder and Fins*. London, U.K.: Springer Science & Business Media, 2006.

[25] S.-H. Ham, M.-I. Roh, H. Lee, J.-W. Hong, and H.-R. Lee, "Development and validation of a simulation-based safety evaluation program for a mega floating crane," *Adv. Eng. Softw.*, vol. 112, pp. 101–116, Oct. 2017.

[26] N. Khaled and N. Chalhoub, "A dynamic model and a robust controller for a fully-actuated marine surface vessel," *J. Vibrat. Control*, vol. 17, no. 6, pp. 801–812, May 2011.

[27] S. Boyd, "Distributed optimization and statistical learning via the alternating direction method of multipliers," *Found. Trends Mach. Learn.*, vol. 3, no. 1, pp. 1–122, 2010.

[28] F. Borrelli, A. Bemporad, and M. Morari, *Predictive Control for Linear and Hybrid Systems*. London, U.K.: Cambridge Univ. Press, 2017.

[29] L. Zhang, S. Zhuang, and R. D. Braatz, "Switched model predictive control of switched linear systems: Feasibility, stability and robustness," *Automatica*, vol. 67, pp. 8–21, May 2016.

[30] Z. Du, R. R. Negenborn, and V. Reppa, "COLREGS-compliant collision avoidance for physically coupled multi-vessel systems with distributed MPC," *Ocean Eng.*, vol. 260, Sep. 2022, Art. no. 111917.

[31] L. Chen, Y. Huang, H. Zheng, H. Hopman, and R. Negenborn, "Cooperative multi-vessel systems in urban waterway networks," *IEEE Trans. Intell. Transp. Syst.*, vol. 21, no. 8, pp. 3294–3307, Aug. 2020.

[32] A. Haseltalab and R. R. Negenborn, "Model predictive maneuvering control and energy management for all-electric autonomous ships," *Appl. Energy*, vol. 251, Oct. 2019, Art. no. 113308.
[33] N. Bialystocki and D. Konovessis, "On the estimation of ship's fuel consumption and speed curve: A statistical approach," *J. Ocean Eng. Sci.*, vol. 1, no. 2, pp. 157–166, Apr. 2016.

Zhe Du received the M.Sc. degree in transport information engineering and control from the Wuhan University of Technology, Wuhan, China, in 2018, and the Ph.D. degree in cooperative control of autonomous multivessel systems for floating object manipulation from the Delft University of Technology, Delft, The Netherlands, in 2022.

He is currently an Assistant Professor with the School of Naval Architecture, Ocean and Energy Power Engineering, Wuhan University of Technology. His research interests include cooperative control, multi-vessel systems, distributed control, model-predictive control, and floating object manipulation.

Rudy R. Negenborn received the M.Sc. degree in computer science/intelligent systems from Utrecht University, Utrecht, The Netherlands, in 1998, and the Ph.D. degree in distributed control for networked systems from the Delft University of Technology, Delft, The Netherlands, in 2007.

He is currently a Full Professor of "multimachine operations and logistics" with the Department of Maritime and Transport Technology, Delft University of Technology. His research interests include distributed control, multicontroller systems, model-predictive control, and optimization. He applies the developed theories to address control problems in large-scale transportation and logistics systems.

Vasso Reppa (Member, IEEE) received the Ph.D. degree in electrical and computer engineering from the University of Patras, Patras, Greece, in 2010.

From 2011 to 2017, she was a Research Associate (now Research Affiliate) with the KIOS Research and Innovation Center of Excellence, Nicosia, Cyprus. In 2013, she was awarded the Marie Curie Intra European Fellowship and was a Research Fellow with CentraleSupélec, University of Paris-Saclay, Gif-sur-Yvette, France, from 2014 to 2016. She was a Visiting Researcher with Imperial College London, London, U.K., in 2015, and with The University of Newcastle, Callaghan, NSW, Australia, in 2016. She has been an Assistant Professor with the Department of Maritime and Transport Technology, Delft University of Technology, Delft, The Netherlands, since 2018. She has also been involved in several research and development projects (e.g., INTERREG "AVATAR," H2020 "NOVIMOVE," NWO "READINESS," and Marie Curie ITN "AUTO-Barge"). Her current research interests include multiagent fault diagnosis and fault-tolerant control, cooperative control, adaptive learning, observer-based estimation, and applications of autonomous systems in (waterborne) transport and smart buildings.